

Real-Time Optimal Embedded Control of a Double Inverted Pendulum

Luis A. Rios-Noreña, Juan S. Velez-Ramirez, Eduardo Giraldo

Abstract—In this work, an under-actuated two degrees of freedom planar robot called pendubot is controlled by using a real-time embedded discrete linear quadratic regulator. The proposed approach is validated over a real prototype using a C2000 F28379d Delfino dual-core processor. Two scenarios are evaluated: the double inverted pendulum in a top position and the inverted pendulum in a middle position. The double inverted pendulum proposed control approach is compared with a state-of-the-art state feedback control strategy. The mean-square-error and integral-time-absolute-error are used to evaluate the controller's performance. As a result, the discrete linear-quadratic embedded real-time controller outperformed the state-of-the-art controllers.

Index Terms—Embedded control, optimal control, real-time, pendubot.

I. INTRODUCTION

THE development of dedicated real-time microcontrollers for control tasks has improved the design of autonomous systems [1], [2]. Several works have used the structure of embedded controllers to control power electronics as well as mechatronic systems [3], [4], [5]. In [6], a synchronous Buck converter real-time fractional controller is evaluated using an embedded structure over a C2000 Texas Instruments microcontroller. In addition, in [7] a HIL simulation by considering a magnetic levitation system with an Arduino microcontroller is also considered for time-varying reference tracking. In [8] an embedded centralized and decentralized controllers of a microgrid are assessed over a Hardware-In-the-Loop (HIL) structure also using a real-time design, and a similar approach is presented in [9] for a modified PID configuration over a HIL validation structure.

In this work, real-time embedded control is analyzed over a pendubot. The pendubot is a highly complex under-actuated system that allows the validation of real-time linear and nonlinear control techniques [10]. The pendubot is a two-link under-actuated planar robot with a single actuator at the first joint [11], which is a typical example of MIMO under-actuated robots. This system allows experimental validation of several control techniques in real-time due to the nature of its construction and its inherent dynamics [12], [13]. In fact, due to its construction, the pendubot system also allows several equilibrium points, which increases the possibility to evaluate real-time embedded controllers [14].

Manuscript received August 25, 2021; revised March 3, 2022.

Luis A. Rios-Noreña is a Researcher at the Research group in Automatic Control, Universidad Tecnológica de Pereira, Pereira, Colombia. E-mail: luis.rios@utp.edu.co

Juan S. Velez-Ramirez is a Researcher at the Research group in Automatic Control, Universidad Tecnológica de Pereira, Pereira, Colombia. E-mail: jusever@utp.edu.co

Eduardo Giraldo is a full professor at the Department of Electrical Engineering, Universidad Tecnológica de Pereira, Pereira, Colombia. Research group in Automatic Control. E-mail: egiraldos@utp.edu.co

Several techniques are evaluated over the pendubot due to its nonlinear nature. For example, in [15] a set of hybrid control techniques are applied and evaluated over the pendubot, where the partial and optimal feedback strategies are considered. In [16], a fuzzy control method is applied over the pendubot, where the state feedback control is extended to dual fuzzy PD control. Another hybrid optimal approach is presented in [17], where the discrete mechanics and optimal control achieve the feedforward control by optimizing the trajectories for energy consumption and transition time.

In this work, a discrete optimal control is proposed in terms of the linear quadratic regulator. The optimal control is evaluated over a double inverted pendulum system by using a C2000-based Texas Instruments Digital Signal Controller. The proposed approach is compared with state-of-the-art state feedback methods and a full state feedback controller. The proposed approach is also evaluated by considering mean-squared-error (MSE) and integral-time absolute-error (ITAE) criteria. This paper is organized as follows: In section II is presented the theoretical framework. In section IV are presented the experimental setup, results, and discussions, and finally, in section V are presented the final remarks and future works.

II. THE PENDUBOT

Figure 1 shows the mechatronics control kit produced by Quanser configured as the pendubot. This device could be described as a nonlinear under-actuated planar robot [18], with a DC motor controlling two arms connected by a non-controlled articulation, with the angle feedback provided by two digital encoders. The control task is to maintain the balance of the second arm on the unstable equilibrium point on the top of the articulation, which leads to two different feedback configurations.

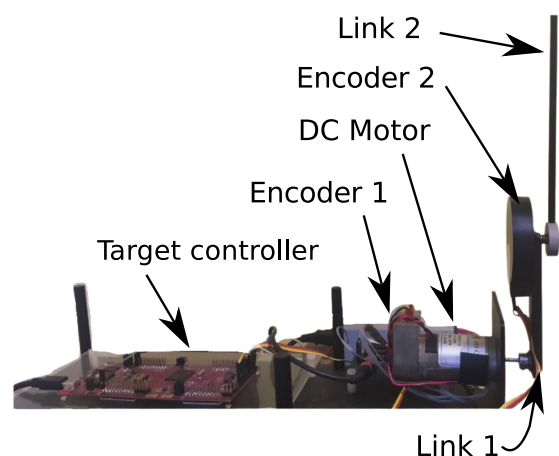


Fig. 1. Side perspective schematic of the pendubot

The mathematical model of the pendubot is inferred from the dynamics of its simplified free-body diagram, as shown in Fig. 2. The pendubot can be considered as *double inverted pendulum* with two operational points: the pendulum in a top position (both arms in the up position), and the pendulum in a middle-position (the first arm up-side-down, and the second arm in the up position).

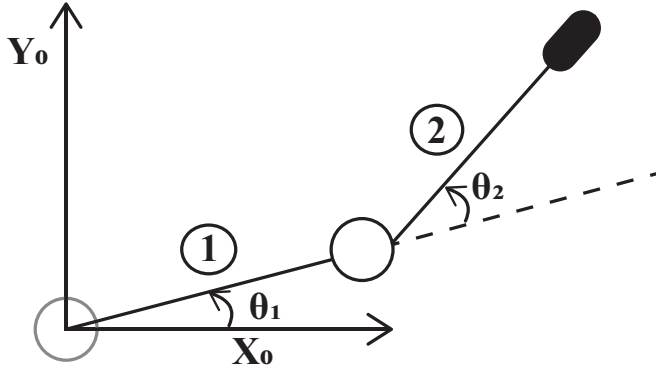


Fig. 2. Simplified free-body diagram of the pendubot.

The dynamics of the pendubot can be obtained by applying the Lagrangian dynamics of (1), as proposed in [19].

$$\tau = D(q)\ddot{q} + C(q, \dot{q})\dot{q} + g(q) \quad (1)$$

where τ is the vector of torque applied to the links, and q is the vector of joint angle positions such that the mass or inertia matrix D is given by expression (2), as described in [20].

$$D(q) = \begin{bmatrix} d_{11} & d_{12} \\ d_{21} & d_{22} \end{bmatrix} \quad (2)$$

being

$$\begin{aligned} d_{11} &= m_1 l_{c1}^2 + m_2 (l_1^2 + l_{c2}^2 + 2l_1 l_{c2} \cos q_2) + I_1 + I_2 \\ d_{12} &= d_{21} = m_2 (l_{c2}^2 + l_1 l_{c2} \cos q_2) + I_2 \\ d_{22} &= m_2 l_{c2}^2 + I_2 \end{aligned}$$

and the Coriolis and centrifugal force matrix C lead by (3)

$$C(q, \dot{q}) = \begin{bmatrix} h\dot{q}_2 & h\dot{q}_2 + h\dot{q}_1 \\ -h\dot{q}_1 & 0 \end{bmatrix} \quad (3)$$

where

$$h = -m_2 l_1 l_{c2} \sin q_2$$

and the gravity matrix g (4):

$$g(q) = \begin{bmatrix} \phi_1 \\ \phi_2 \end{bmatrix} \quad (4)$$

and

$$\begin{aligned} \phi &= (m_2 l_{c1} + m_2 l_1)g \cos q_1 + m_2 l_{c2} g \cos(q_1 + q_2) \\ \phi &= m_2 g l_{c2} \cos(q_1 + q_2) \end{aligned}$$

A description of the model constants are listed below:

- m_1 , the total mass of link one.
- l_1 , the length of link one.
- l_{c1} , the distance to the center of mass of link 1.
- I_1 , the moment of inertia of link one about its centroid.
- m_2 , the total mass of link two.
- L_{c2} , the distance to the center of mass of link 2.

- I_2 , the moment of inertia of link two about its centroid,
- g , the gravity acceleration.

The nonlinear dynamic model is obtained by applying the inversion property of the mass matrix D described in [19], leading expression (5), as follows:

$$\begin{bmatrix} \ddot{q}_1 \\ \ddot{q}_2 \end{bmatrix} = D(q)^{-1}\tau - D(q)^{-1}C(q, \dot{q})\dot{q} - D(q)^{-1}g(q) \quad (5)$$

where the system states are defined by:

$$\begin{aligned} x_1 &= q_1, x_2 = \dot{q}_1, x_3 = q_2, x_4 = \dot{q}_2 \\ \dot{x}_1 &= x_2 \\ \dot{x}_2 &= \ddot{q}_1 \\ \dot{x}_3 &= x_4 \\ \dot{x}_4 &= \ddot{q}_2 \end{aligned}$$

and

$$\underline{x} = [q_1 \quad \dot{q}_1 \quad q_2 \quad \dot{q}_2]^T$$

Note that the set of equations (5) describes two second-order nonlinear differential equations. The model must be linearized around the operation equilibrium points to apply the optimal control theory. The particular case of the inverted pendulum leads to the conclusion that the equilibrium values from the model states and control signal are equal to zero [19].

By using the approximation of the Taylor series, given in expression (6), the linearized system is described as the following set of equations:

$$f_a(x, u) = f_a(x_r, u_r) + \left. \frac{\partial f}{\partial x} \right|_{x_r, u_r} (x - x_r) + \left. \frac{\partial f}{\partial u} \right|_{x_r, u_r} (u - u_r) \quad (6)$$

where the partial derivative of the state vector x is computed by using:

$$\frac{\partial f}{\partial x} = \begin{bmatrix} 0 & 1 & 0 & 0 \\ \frac{\partial f_2}{\partial x_1} & 0 & \frac{\partial f_2}{\partial x_3} & 0 \\ 0 & 0 & 0 & 1 \\ \frac{\partial f_4}{\partial x_1} & 0 & \frac{\partial f_4}{\partial x_3} & 0 \end{bmatrix}$$

and the open-loop input is determined by:

$$\frac{\partial f}{\partial u} = \begin{bmatrix} 0 \\ \frac{\partial f_2}{\partial u} \\ 0 \\ \frac{\partial f_4}{\partial u} \end{bmatrix}$$

The linearized model of the pendubot is lead by expression (II):

$$\begin{aligned} \frac{d}{dt} \begin{bmatrix} q_1 \\ \dot{q}_1 \\ q_2 \\ \dot{q}_2 \end{bmatrix} &= \begin{bmatrix} 0 & 1 & 0 & 0 \\ \frac{(\theta_2 \theta_4 - \theta_3 \theta_5)g}{\theta_1 \theta_2 - \theta_3^2} & 0 & \frac{-\theta_3 \theta_5 g}{\theta_1 \theta_2 - \theta_3^2} & 0 \\ 0 & 0 & 0 & 1 \\ \frac{\theta_5 g (\theta \theta_1 + \theta_3) - \theta_4 g (\theta_2 + \theta_3)}{\theta_1 \theta_2 - \theta_3^2} & 0 & \frac{\theta_5 g (\theta_1 + \theta_3)}{\theta_1 \theta_2 - \theta_3^2} & 0 \end{bmatrix} \begin{bmatrix} q_1 \\ \dot{q}_1 \\ q_2 \\ \dot{q}_2 \end{bmatrix} \\ &+ \begin{bmatrix} 0 \\ \frac{\theta_2}{\theta_1 \theta_2 - \theta_3^2} \\ 0 \\ \frac{-\theta_2}{\theta_1 \theta_2 - \theta_3^2} \end{bmatrix} \tau_1 = AY + B\tau_1 \quad (7) \end{aligned}$$

An identification process that allows the estimation of the system constants is used, as shown in [21]. As a result, two different models are obtained according to the angular position of the first link: Top position and middle position.

1) *Top position*: The unstable equilibrium point of the second link is reached with the first link is located at a 90° angle with respect to the coordinate plane. The pendubot in the top-position scenario is shown in Fig. 3.

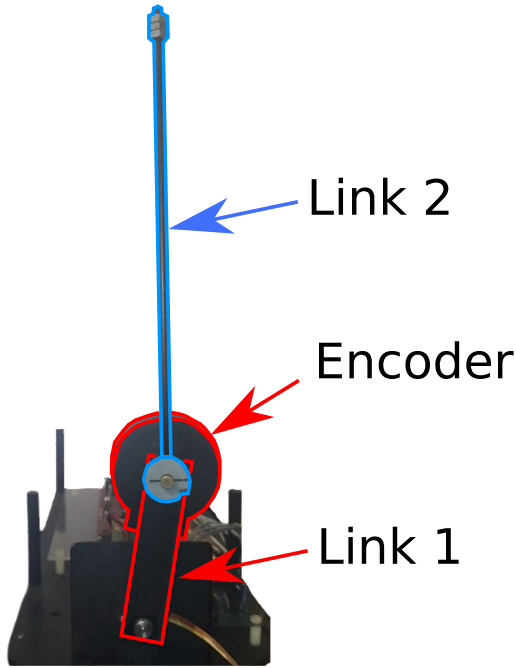


Fig. 3. The pendubot system in the Top-position.

A linear estimated representation of the system in space-state is therefore obtained by following the general form given by (8). This procedure leads to the expression (10), as described in [20].

$$\dot{x} = Ax(t) + Bu(t) \quad (8)$$

being

$$A = \begin{bmatrix} 0 & 1 & 0 & 0 \\ 153 & 0 & -43.87 & 0 \\ 0 & 0 & 0 & 1 \\ -174.4 & 0 & 126.71 & 0 \end{bmatrix} \quad (9)$$

$$B = \begin{bmatrix} 0 \\ 25.738 \\ 0 \\ -39.37 \end{bmatrix} \quad (10)$$

It is necessary to clarify that the lack of a swing up strategy forces to start the model with initial condition (x_i) in a top position. This initial position must satisfy: $x_i = [\frac{\pi}{2}, 0, 0, 0]^T$.

2) *Middle position*: The unstable equilibrium point of the second link is reached with the first link has -90° with respect to the coordinate plane. The pendubot in the middle-position scenario is shown in Fig. 3.

Equation (11) is obtained through a linear estimation of the model constants, as presented in [20], as follows:

$$A = \begin{bmatrix} 0 & 1 & 0 & 0 \\ -153 & 0 & 43.87 & 0 \\ 0 & 0 & 0 & 1 \\ 131.6 & 0 & 38.96 & 0 \end{bmatrix} \quad B = \begin{bmatrix} 0 \\ 25.738 \\ 0 \\ -12.107 \end{bmatrix} \quad (11)$$

The initial conditions x_i for the middle position operational point are given by $x_i = -[\frac{\pi}{2}, \pi, 0, 0]^T$.

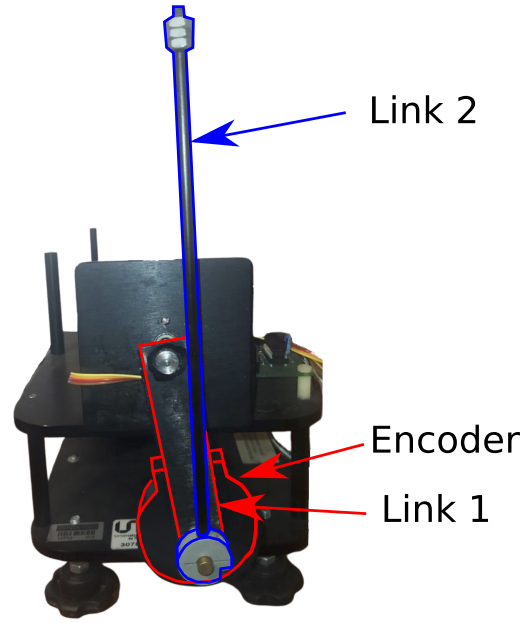


Fig. 4. The pendubot system in the middle-position.

III. OPTIMAL CONTROL

A. Linear Quadratic Regulator (LQR)

The LQR is a well-known method that provides optimally controlled feedback gains to enable closed-loop stability and high-performance design. This allow the solution of the matrix Difference Riccati Equation (DRE) of (12), as proposed in [22].

$$\dot{\mathbf{P}}(k) = \mathbf{A}'(k)\mathbf{P}(k+1)[\mathbf{I} + \mathbf{E}(k)\mathbf{P}(k+1)]^{-1}\mathbf{A}(k) + \mathbf{Q}(k) \quad (12)$$

with final condition $\mathbf{P}(k = k_f) = \mathbf{F}(k_f)$, where $\mathbf{E}(k) = \mathbf{B}(k)\mathbf{R}^{-1}(k)\mathbf{B}'(k)$.

The optimal state is solved for $x^*(k)$ from (13), as follows:

$$\mathbf{x}^*(k+1) = [\mathbf{A}(k) - \mathbf{B}(k)\mathbf{L}(k)]\mathbf{x}^*(k) \quad (13)$$

with initial condition $\mathbf{x}(k_0) = \mathbf{x}_0$, where

$$\mathbf{L}(k) = \mathbf{R}^{-1}(k)\mathbf{B}'(k)\mathbf{A}^{-T}(k)[\mathbf{P}(k) - \mathbf{Q}(k)]. \quad (14)$$

and the optimal control $\mathbf{u}^*(k)$ is obtained from

$\mathbf{u}^*(k) = -\mathbf{L}(k)\mathbf{x}^*(k)$ where, $\mathbf{L}(k)$ is the Kalman gain (14).

The optimal performance index from (15) is obtained as

$$J^* = \frac{1}{2}\mathbf{x}'^*(k)\mathbf{P}(k)\mathbf{x}^*(k) \quad (15)$$

B. Constraint matrix parameters

The values in the matrix (16) and (17) are built-in by the plant manufacturer. The constraint parameters Q and R are used to get the LQR behavior controller during the running time. The constraint parameters are defined as follows:

$$Q = \begin{bmatrix} 0.05 & 0 & 0 & 0 \\ 0 & 850 & 0 & 0 \\ 0 & 0 & 10000 & 0 \\ 0 & 0 & 0 & 0 \end{bmatrix} \quad (16)$$

and

$$R = 100 \quad (17)$$

According to the LQR method, the state feedback vector is given by $K = (R + B^T P B)^{-1} B^T P A$, where $P = P^T \succ 0$ is the unique solution of the Control Algebraic Riccati Equation (CARE). The optimal state-feedback $u_k = -K x_k$ ensures the asymptotic stability of the closed-loop system. The feedback vector K is computed by the built-in Matlab function $lqr(A, B, Q, R, Ts)$ [23].

The Matlab function “lqr” can be used to derive optimal control gains for a discrete controller. Using a sampling period of 5ms, the optimal gains are defined in (18) and (19).

1) *Top-position:*

$$K = [-127.6356 \quad -21.2588 \quad -125.2540 \quad -15.9731] \quad (18)$$

2) *Middle-position:*

$$K = [98.8684 \quad 9.9684 \quad 116.5689 \quad 14.8456] \quad (19)$$

IV. RESULTS

A. Experimental Setup

In order to evaluate the proposed approach in a real-time implementation, a MATLAB/Simulink environment is used. It is worth noting that by using Code Composer Studio the controllers are compiled and uploaded to the Texas Instruments F28379d Launchpad depicted in Fig. 5. Serial communication with the processor allows a real-time performance evaluation. A relevant feature of this setup is the supervision stage that allows online handling of the control parameters, simplifying the study of the system dynamics under different control constants. This configuration also eases the offset setting at the operation points.



Fig. 5. Texas Instruments F28379d Launchpad connected to the encoders and motor driver.

A connection diagram that shows the experimental setup is depicted in Fig. 6.

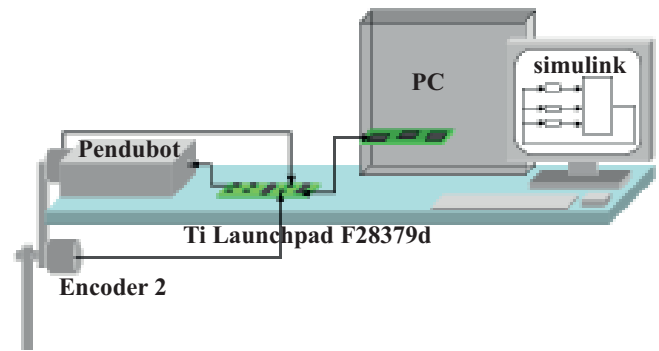


Fig. 6. Experimental setup

B. Classical full-state feedback control

In order to validate the proposed optimal control algorithms, two full-state feedback controllers are designed experimentally, each related to the respective operating mode. The controllers are tuned experimentally with the support of the information provided by Quanser about the constant values of the mechatronic Kit. The selected discrete poles of the model are shown in (20).

$$P = [0.9324 \quad 0.9282 \quad 0.9231 \quad 0.9185] \quad (20)$$

The built-in *eigenvalues relocation toolbox* of MATLAB is used to quantify the controllers gains.

1) *Top-position:*

$$K = [-182.9053 \quad -28.1978 \quad -158.7556 \quad -19.8816] \quad (21)$$

2) *Middle-position:*

$$K = [119.2740 \quad 11.5218 \quad 158.5817 \quad 19.8608] \quad (22)$$

C. Results

The evaluation of the prototype system is performed by considering the embedded real-time controller over a Texas Instruments C2000 Delfino F28379d Launchpad. The analysis is performed under the two discussed scenarios: first scenario -pendulum in the middle position, second scenario -pendulum in top position.

Figure 7 shows a comparison analysis between the LQR and Full-state-feedback controllers for the Link 1 in the Top-Position.

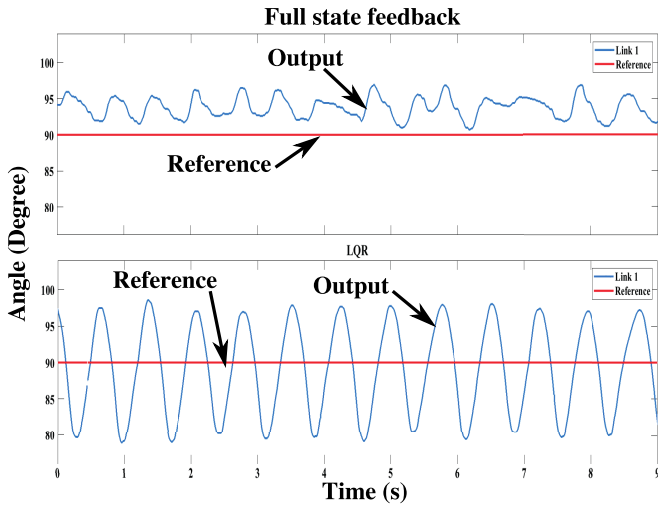


Fig. 7. Performance analysis of the Link 1 in Top-Position for LQR and Full-state-feedback controllers

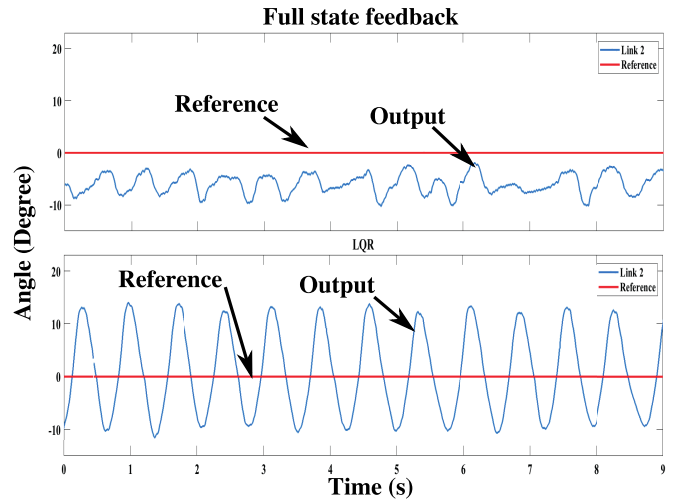


Fig. 9. Performance analysis of the Link 2 in Top-Position for LQR and Full-state-feedback controllers

A detailed analysis of Fig. 7 is presented in Fig. 8.

A detailed analysis of Fig. 9 is presented in Fig. 10.

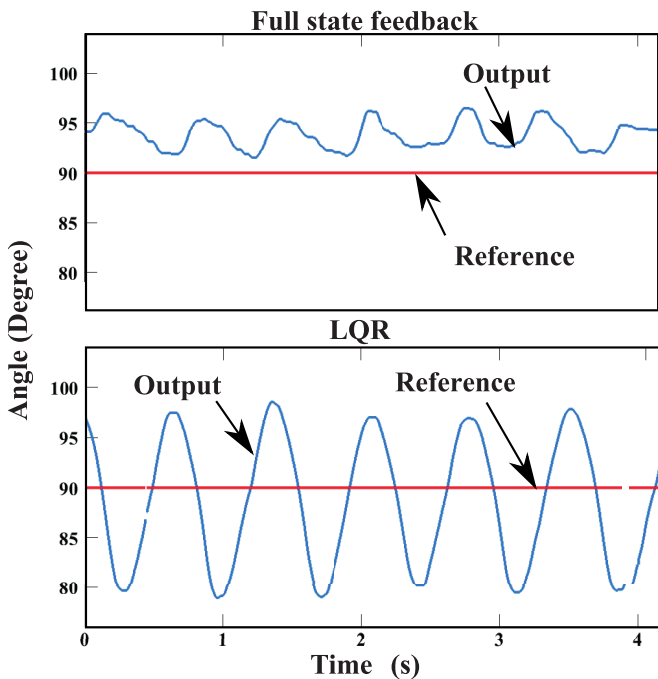


Fig. 8. Detailed performance analysis of the Link 1 in Top-Position for LQR and Full-state-feedback controllers

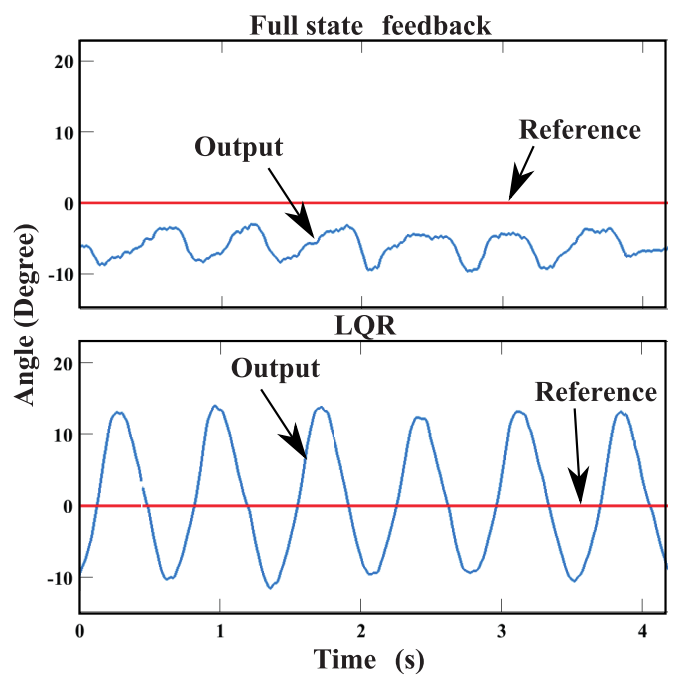


Fig. 10. Detailed performance analysis of the Link 2 in Top-Position for LQR and Full-state-feedback controllers

Figure 9 shows a comparison between the LQR and Full-state-feedback controllers for the Link 2 in the Top-Position.

Figure 11 shows a comparison between the LQR and Full-state-feedback controllers for the Link 1 in the Middle-Position.

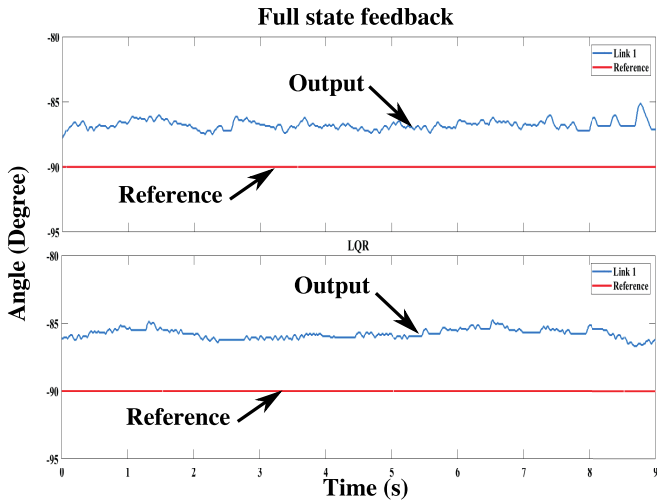


Fig. 11. Performance analysis of the Link 1 in Middle-Position for LQR and Full-state-feedback controllers

A detailed analysis of Fig. 11 is presented in Fig. 12.

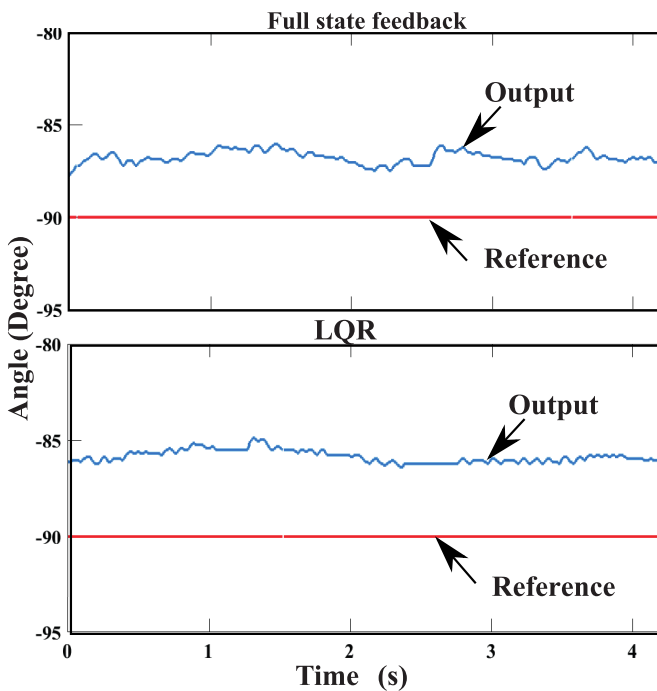


Fig. 12. Detailed performance analysis of the Link 1 in Middle-Position for LQR and Full-state-feedback controllers

Figure 13 shows a comparison between the LQR and Full-state-feedback controllers for the Link 2 in the Middle-Position.

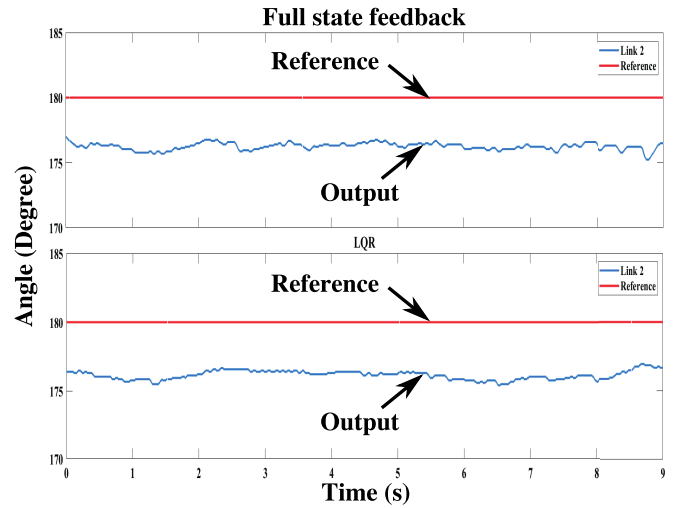


Fig. 13. Performance analysis of the Link 2 in Middle-Position for LQR and Full-state-feedback controllers

A detailed analysis of Fig. 13 is presented in Fig. 14.

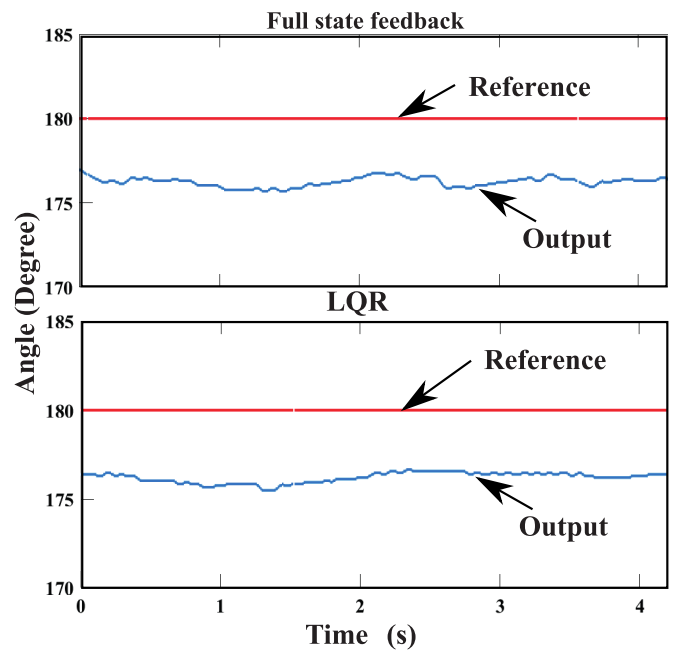


Fig. 14. Detailed performance analysis of the Link 2 in Middle-Position for LQR and Full-state-feedback controllers

The embedded controller is developed in Matlab-Simulink by using a block-diagram structure. This embedded controller has several stages as follows: a signal conditioning stage where the encoder signal is converted to the angle position. A second stage, where the embedded controller is implemented, by including the optimal control approach by linear quadratic methods. And a final stage, where control signal is scaled to the duty cycle range of the PWM.

Figure 15 shows the block-diagram of the embedded controller for the pendubot in a top-position scenario.

Figure 16 shows the block-diagram of the embedded controller for the pendubot in a middle-position scenario.

D. Error comparisons

This section presents a comparative analysis of the performance between the Full-state-feedback (FSF) and

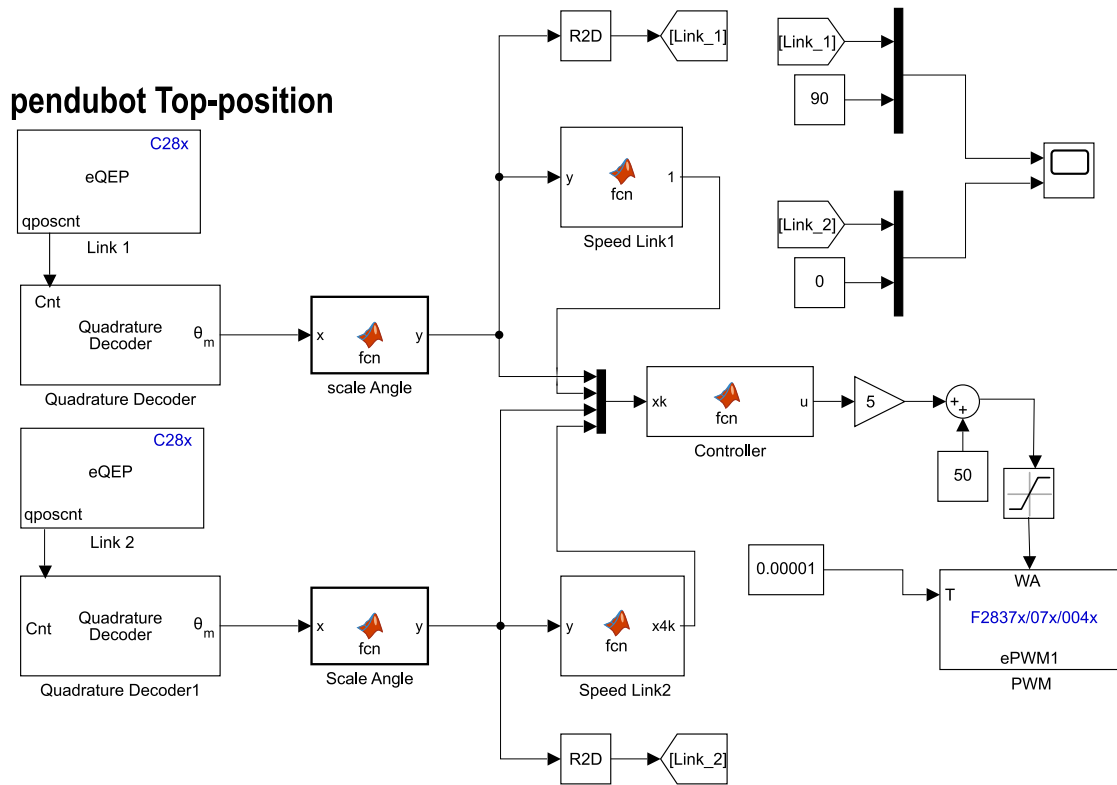


Fig. 15. Block diagram of the embedded controller for a pendubot in a top-position scenario

the Linear-Quadratic Regulator (LQR) controller. The comparison analysis is performed by considering execution time in order to know the joint angle reference tracking for each link of the pendubot. Two error measures are used: the MSE and the ITAE.

The values of MSE for the top-position scenario are shown in Table I.

TABLE I
MSE OF THE TOP-POSITION SCENARIO

Link 1		Link 2	
FSF	LQR	FSF	LQR
1.0933×10^6	5.5205×10^5	2.4828×10^6	9.6117×10^5

Table II shows the values of ITAE for the top-position scenario.

TABLE II
ITAE OF THE TOP-POSITION SCENARIO

Link 1		Link 2	
FSF	LQR	FSF	LQR
320.8676	231.4405	476.3491	231.4405

The values of MSE for the middle-position scenario are shown in Table III.

TABLE III
MSE OF THE MIDDLE-POSITION SCENARIO

Link 1		Link 2	
FSF	LQR	FSF	LQR
2.3422×10^6	2.1426×10^6	2.6174×10^6	2.0390×10^6

Table IV shows the values of ITAE for the middle-position scenario.

TABLE IV
ITAE OF THE MIDDLE-POSITION

Link 1		Link 2	
FSF	LQR	FSF	LQR
1.4105×10^3	1.3154×10^3	1.4449×10^3	1.3638×10^3

V. CONCLUSIONS

This work presents an embedded real-time optimal control in discrete time, and it is validated over a double inverted pendulum system. The obtained results show that the gain provided by LQR has significant robustness to applied disturbances since the system effectively returns to the equilibrium point. On the other hand, the full-state-feedback controller is usually more susceptible to disturbances and therefore an additional control strategy is required to reach the equilibrium point. It is worth mentioning that the real-time evaluation of the proposed controller by using a C2000 F28379d system, can be extended to the evaluation of several controllers in real-time. Therefore, as future work, several controllers will be evaluated over the prototype by using the aforementioned experimental setup.

REFERENCES

- [1] F. Bormann, E. Braune, and M. Spitzner, "The c2000 autonomous model car," in *4th European Education and Research Conference (EDERC 2010)*, 2010, pp. 200–204.
- [2] B. Allotta, R. Costanzi, N. Monni, M. Natalini, L. Pugi, and A. Ridolfi, "Fast prototyping of a scaled agv for the testing of stability control for industrial vehicles," in *2014 6th European Embedded Design in Education and Research Conference (EDERC)*, 2014, pp. 202–206.

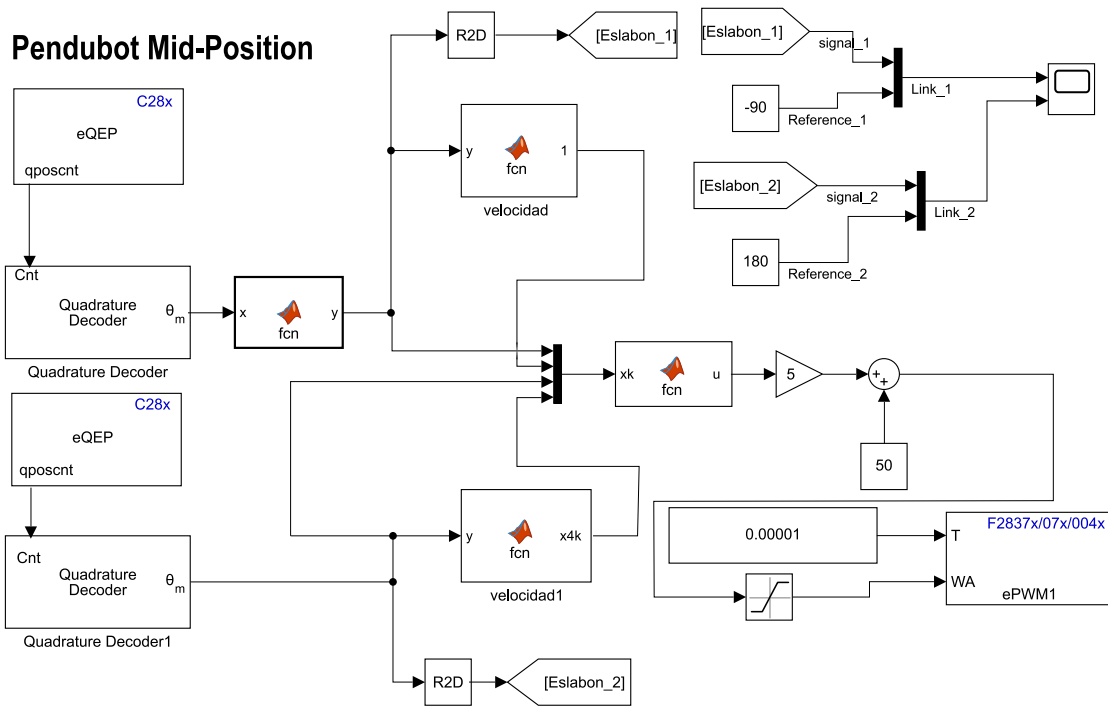


Fig. 16. Block diagram of the embedded controller for a pendubot in a middle-position scenario

- [3] K. N. N. A. Kumar and C. P. Kurian, "Model based control using c2000 microcontroller," in *2014 International Conference on Advances in Energy Conversion Technologies (ICAECT)*, 2014, pp. 13–20.
- [4] R. V. Castelino, S. Jana, and P. K. Biswas, "Analysis of realtime inverter for kite energy system using ti -c2000 microcontroller," in *2018 2nd International Conference on Power, Energy and Environment: Towards Smart Technology (ICEPE)*, 2018, pp. 1–5.
- [5] N. Thodsaporn and V. Kinnares, "Wind turbine simulator equipped with real-time monitoring and user-friendly parameter setup controlled by c2000 microcontroller," in *2020 17th International Conference on Electrical Engineering/Electronics, Computer, Telecommunications and Information Technology (ECTI-CON)*, 2020, pp. 713–716.
- [6] M. Bueno-Lopez and E. Giraldo, "Real-time fractional order pi for embedded control of a synchronous buck converter," *Engineering Letters*, vol. 29, no. 3, pp. 1212–1219, 2021.
- [7] E. Giraldo, "Real-time control of a magnetic levitation system for time-varying reference tracking," *IAENG International Journal of Applied Mathematics*, vol. 51, no. 3, pp. 792–798, 2021.
- [8] M. Bueno-Lopez and E. Giraldo, "Real-time decentralized control of a hardware-in-the-loop microgrid," *IAENG International Journal of Computer Science*, vol. 48, no. 3, pp. 653–662, 2021.
- [9] E. Giraldo, "Real-time modified pid controller over a dc-dc boost converter," *IAENG International Journal of Applied Mathematics*, vol. 51, no. 3, pp. 1–12, 2021.
- [10] S. Rudra and R. K. Barai, "Design of block backstepping based nonlinear state feedback controller for pendubot," in *2016 IEEE First International Conference on Control, Measurement and Instrumentation (CMI)*, 2016, pp. 1–5.
- [11] A.-W. A. Saif, "Strong stabilization of the non-linear pendubot system," in *2015 IEEE 12th International Multi-Conference on Systems, Signals Devices (SSD15)*, 2015, pp. 1–7.
- [12] T. V. Toan, T. T. Ha, and T. V. Do, "Hybrid control for swing up and balancing pendubot system: An experimental result," in *2017 International Conference on System Science and Engineering (ICSSE)*, 2017, pp. 450–453.
- [13] M. Salaj, M. Gulan, and B. Rohal'-Ilkiv, "Pendubot control scheme based on nonlinear mpc and mhe exploiting parallelization," in *2015 IEEE 19th International Conference on Intelligent Engineering Systems (INES)*, 2015, pp. 353–358.
- [14] M. Gulan, M. Salaj, and B. Rohal'-Ilkiv, "Nonlinear model predictive control with moving horizon estimation of a pendubot system," in *2015 20th International Conference on Process Control (PC)*, 2015, pp. 226–231.
- [15] D. Giraldo Buitrago, G. Holguín, and A. Escobar Mejía, "Técnicas híbridas de control aplicadas al pendubot," *Scientia et Technica*, vol. 1, no. 30, ene. 2006. [Online]. Available: <https://revistas.utp.edu.co/index.php/revistaciencia/article/view/6491>
- [16] J.-H. Li, "Dual fuzzy pd control of dsp-based pendubot," in *2011 8th Asian Control Conference (ASCC)*, 2011, pp. 641–646.
- [17] J. Timmermann, S. Khatib, S. Ober-Blöbaum, and A. Trächtler, "Discrete mechanics and optimal control and its application to a double pendulum on a cart," *IFAC Proceedings Volumes*, vol. 44, no. 1, pp. 10 199–10 206, 2011, 18th IFAC World Congress. [Online]. Available: <https://www.sciencedirect.com/science/article/pii/S1474667016452511>
- [18] C. Wei, T. Chai, X. Xin, X. Chen, L. Wang, and Y. H. Chen, "A Signal Compensation-Based Robust Swing-up and Balance Control Method for the Pendubot," *IEEE Transactions on Industrial Electronics*, 2021.
- [19] D. J. Block and M. W. Spong, "mA =For Advancing Mobility and Sea Air and Space, Mechanical Design and Control of the Pendubot," university of Illinois, Illinois, Tech. Rep., 3 1995.
- [20] J. A. C. Meesters, D. Lizarraga, and H. Nijmeijer, "The mechatronics kit: first survey," Technische Universiteit Eindhoven, Eindhoven, Tech. Rep., 11 2004. [Online]. Available: <https://research.tue.nl/en/publications/the-mechatronics-kit-first-survey>
- [21] W. Xu and J. Liu, "Identification of underactuated manipulator based on genetic algorithm," in *IEEE 10th International Conference on Industrial Informatics*, 2012, pp. 653–656.
- [22] D. S. D. S. Naidu, *Optimal control systems*. CRC Press, 2003.
- [23] A. Odry, E. Burkus, and P. Odry, *LQG Control of a Two-Wheeled Mobile Pendulum System*. Hungary: IARIA, 2015.